ISSN 0304-9892 (Print) ISSN 2455-7463 (Online)
www.vijnanaparishadofindia.org/jnanabha
***Jñānābha*, Vol. 53(1) (2023), 3-21**
(Dedicated to Professor G. C. Sharma on His 85^{th} Birth Anniversary Celebrations)

UNSTEADY *MHD* SLIP FLOW OF RADIATING NANOFLUID THROUGH A POROUS MEDIA DUE TO A SHRINKING SHEET WITH CHEMICAL REACTION AND SORET EFFECT

V. K. Jarwal and S. Choudhary
Department of Mathematics, University of Rajasthan, Jaipur, India-302004
E-mail: jarwalvijendrakumar@gmail.com, sumathru11@gmail.com

(*Received: May* 09, 2022; *In format: May* 12, 2022; *Revised: January* 01, 2023; *Accepted: January* 31, 2023)

DOI: https://doi.org/10.58250/jnanabha.2023.53101

Abstract

Numerical investigations are performed to analyze heat and mass transfer in *MHD* (magnetohydrodynamic) nanofluid flow over a shrinking sheet in the presence of thermal radiation and chemical reaction with Soret effect. The transport equations involve the effect of Brownian motion,Thermophoresis, viscous dissipation, suction/injection, partial slip velocity and thermal slip. Using self suitable transformations, the governing equations are reduced to ordinary differential equations, further these equations are solved numerically using Runge-Kutta fourth order method with shooting technique. This study reveals that the governing parameters, namely, magnetic field parameter, thermal radiation parameter, chemical reaction parameter, velocity slip parameter etc., have major effects on velocity, temperature, concentration, skin friction coefficient and Nusselt number. The study admits that concentration rises with an increase in the Soret number. Numerical results are discussed with the assistance of graphs. The present problem has multiple applications in polymer, chemical and metallurgical industries such as formation of metallic and glass sheets.

2020 Mathematical Sciences Classification : 76D05 ,76D10, 76S05, 76W05, 80A21, 80A32.

Keywords: Nanofluid; *MHD* flow; Thermal radiation; Viscous dissipation; Chemical reaction; Slip and Convective boundary conditions; Soret effect.

1 Introduction

Nanofluid is mix suspension of nanometer sized solid particle (*Cu*, *Al*, *Ag*, etc) in base fluid such as water, oil and ethylene glycol, which is first introduced by Choi [6]. Nanofluids have different properties that make them potentially useful for many applications in heat transfer including microelectronics, fuel cells, cancer therapy, domestic refrigerator, pharmaceutical processes and hybrid-power engines. Nanofluids also have some biomedical applications, like in antibacterial and drug delivery. It also has biotechnological applications like nano fibers, nanoparticles, nanowires and nanostructures. Crane [5] initially examined fluid flow past a stretching sheet. An investigation is carried out by Makinde and Aziz [17] on "boundary layer flow of a nanofluid past a stretching sheet with a convective boundary condition". Electric field effect on nanofluid in an enclosure with sinusoidal wall under convective heat transfer was investigated by Sheikholeslami et al. [33]. Various researchers [3, 9, 15, 16, 24, 28] have presented the study of fluid moving over a nonlinear stretching sheet. A non-homogeneous model was presented by Buongiorno [4] to understand the convective transport phenomena in nanofluid. Brownian motion and thermophoresis are found most important in these studied. To analyze the natural convection boundary-layer flow of a nanofluid past a vertical plate, a revised model was presented by Kuznetsov and Nield [14].

The study of magnetic field effect has various impotrant applications in engineering and industry, for instance streamlined expulsion of plastic sheet, glass blowing, metal turning and condensation process of metallic plate in a cooling bath. Magnetic field plays an important role in geophysics, for example controlling heat transfer of different nanofluids and paper production also. Exact solution for *MHD* flow equation of fluid over a shrinking sheet was given by Fang and Zhang [11]. Prasad et al. [20] studied the influence of temperature-dependent fluid properties on the hydro-magnetic flow and heat transfer over a stretching sheet. Free convection flow of magnetohydrodynamics (*MHD*) nanofluid over an infinite flat plate was studied by Hamad et al. [13]. The *MHD* slip flow of Maxwell nanofluid over an exponentially stretching plane was

analyzed by Reddy et al. [26]. Sheikholeslami and Rashidi [32], Sheikholeslami and Ganji [31] studied magnetic field effect on Ferro fluids flow and heat transfer. Daniel et al. [8] carried out an investigation on the electrical *MHD* nanofluid flow over a nonlinear stretching/shrinking sheet. "Finite element simulation of unsteady *MHD* transport phenomena on a stretching sheet in a rotating nanofluid" was discussed by Rana et al. [27]. At present, much attention has been paid to working in the presence of magnetic field effect.

When high temperature are encountered, the study of radiation heat transfer plays an important role in the field of equipment designing [30]. At extremely high-temperature levels, thermal radiation plays an important role in operating the devices in the space technology. Hady et al. [12] and Pal et al. [19] investigated viscous flow of a radiative nanofluid and heat transfer over a nonlinearly stretching/shrinking sheet. In-compressible water based nanofluid flow in the presence of transverse magnetic field with thermal radiation and buoyancy effect was investigated by Rashidi et al. [25]. In recent years, combined heat and mass transfer problem with chemical reaction received significant attention in many processes of interst in Engineering like as drying, evaporation at the surface of a water body, flow in a desert cooler and energy transfer in a wet cooling tower. Sandeep and Sulochana [34] investigated *MHD* flow of nanofluid over a permeable stretching/shrinking sheet with suction/injection. Combined effect of chemical reaction and magnetic field over non-linear stretching sheet was investigated by Awang [2] using Adomain decomposition method (ADM). Anwar et al. [1] studied heat generation/absorption effect on *MHD* flow of a nanofluid over porous stretching sheet with chemical reaction. Effect of chemical reaction and thermal radiation on *MHD* nanofluid flow over non-linear stretching sheet was discussed by Ramya et al. [22].

It is assumed that the velocity of the fluid particles reltive to the solid boundary is zero but the characteristics are different in case of micro and nano-scale fluid flow. Navier [18] first discussed the importance of slip boundary condition, which state that fluid velocity is proportional to shear stress at boundary. *MHD* nanofluid boundary layer slip flow over vertical stretching sheet with non-uniform heat generation/absorption was investigated by Das et al. [7]. *MHD* viscous nanofluid flow and heat transfer over a non-linearly slippery stretching sheet with heat generation/absorption and suction/injection was studied by Ramya et al. [23].

In a system with flowing fluid , dissimilar particles react in different ways to alter temperature, then this thermodynamics trend/phenomena is called the Soret effect. The mass flux can be generated both by the temperature and concentration gradients. Mass fluxes generated by temperature gradients are called the Soret effect. This effect is very important in the operation of solar ponds, the transportation across biological membranes induced by small thermal gradients in living creatures and micro-structure of seas and oceans. This effect is also useful in design and operation of dryers. The Soret effect related to the parting of isotopes and in the combination of gases with small molecular weight (H_2, He) and the average molecular weight (N_2, air) was highlighted by Eckert and Drake [10]. The impact of the Soret effect on stagnation-point flow past a sheet in a nanofluid with non-Darcy porous medium was studied by Reddy et al. [29]. Suneetha et al. [35] presented the Navier slip condition on time-dependent radiating nanofluid with the Soret effect.

In view of above literature survey and development of research in nanofluids, it is revealed that *MHD* slip flow of radiating nanofluids through a porous media with thermal slip in the presence of chemical reaction and Soret effect has not been studied yet, therefore our main aim in the present work is to investigate this aforesaid problem. The governing boundary layer equations are transformed as ordinary differential equations ($ODE's$) using similarity variables which are then solved numerically using fourth order Runge-Kutta method with shooting technique. The influence of various parameters on heat transfer characteristics and the flow field are explored and depicted through graphs or tables.

Nomenclature

A	Unsteadiness parameter	T	Temperature of the nanofluid (K)
B	Magnetic field strength	T_w	Wall temperature(K)
C	Concentration of the nanofluid	T_∞	Ambient temperature (K)
Cf_x	Local skin friction coefficient	T_m	Mean nanofluid temperature (K)
Cr^*	Chemical reaction parameter	u, v	Velocity components (m/s)
C_∞	Ambient Concentration	v_0	Suction velocity (m/s)
C_p	Specific heat at constant pressure	x, y	Cartesian coordinates (m)
D_B	Brownian diffusion coefficient (kg/ms)		
D_m	Mass diffusivity		
D_T	Thermophoretic diffusion coefficient (kg/msK)		*Greek symbols*
Ec	Eckert number	ρ	Density (kg/m^3)
f	Dimensionless stream function	α	Thermal diffusivity (m^2/s)
Ha^2	Magnetic field parameter	κ	Thermal conductivity (m^2/s)

K^*	Permeability parameter	μ	Dynamic viscosity (kg/ms)
K_T	Thermal diffusion ratio	ϕ	Dimentionless concentration
K_0	Permeability of the porous medium (m^2)	δ	Thermal slip parameter
N_1	Thermal slip factor (m)	λ^*	Velocity slip parameter
Le	Lewis number	χ	Shrinking parameter
L_1	Velocity slip factor (m)	ν	Kinematic viscosity (m^2/s)
Nb	Brownian motion parameter	σ	Electric conductivity$(Kg^{-1}m^{-3}t^3A^2)$
Nt	Thermophoresis parameter	ψ	Stream function
Nu_x	Local Nusselt number	η	Similarity variable
Pr	prandlt number	θ	Dimentionless temperature
Q_0	Heat generation coefficient (W/m^2K)		
Q^*	Heat generation parameter		
R	Radiation parameter		*Subscript*
S	Suction parameter	f	Base fluid
Sr	Soret number	np	Nanoparticle
t	Time (s)	∞	Condition at infinity

2 Mathematical Formulation

We consider an unsteady, laminar, incompressible, two-dimensional boundary layer flow of an electrically conducting nanofluid. The flow behavior is examined along nonlinear shrinking sheet under the influence of magnetic field, nonlinear thermal radiation, chemical reaction, Soret effect and thermal slip boundary conditions. Fig. 2.1 shows the flow configuration in which x-axis is taken along the sheet and y-axis perpendicular to the sheet.

The sheet expands/contracts in the x-direction with a velocity $u_w(x,t) = \frac{ax^m}{1-\lambda t}$, where a and λ are constants, $m(\geq 1)$ is a power index and velocity across the wall is $v_w(x,t) = \frac{v_0}{\sqrt{(1-\lambda t)}} x^{\frac{(m-1)}{2}}$. The time dependent magnetic field of variable intensity $B(x,t)$ is assumed to be applied upright to the sheet. Initially the wall temperature T_w is assumed constant at the shrinking sheet. The ambiant fluid temperature T_∞ is considered less than to sheet's temperature T_w.

Bases on the boundary layer approximation, the governing equations of momentum, thermal energy and concentration [21] can be written as

$$\frac{\partial u}{\partial x} + \frac{\partial v}{\partial y} = 0, \tag{2.1}$$

$$\frac{\partial u}{\partial t} + u\frac{\partial u}{\partial x} + v\frac{\partial u}{\partial y} = \nu_f \frac{\partial^2 u}{\partial y^2} - \frac{\sigma}{\rho_f} B^2 u - \frac{\mu_f}{\rho_f K} u, \tag{2.2}$$

$$\frac{\partial T}{\partial t} + u\frac{\partial T}{\partial x} + v\frac{\partial T}{\partial y} = \alpha_f \frac{\partial^2 T}{\partial y^2} - \frac{\partial q_r}{\partial y} + \quad \tau\left[D_B\left(\frac{\partial C}{\partial y}\right)\left(\frac{\partial T}{\partial y}\right) + \left(\frac{D_T}{T_\infty}\right)\left(\frac{\partial T}{\partial y}\right)^2\right] +$$

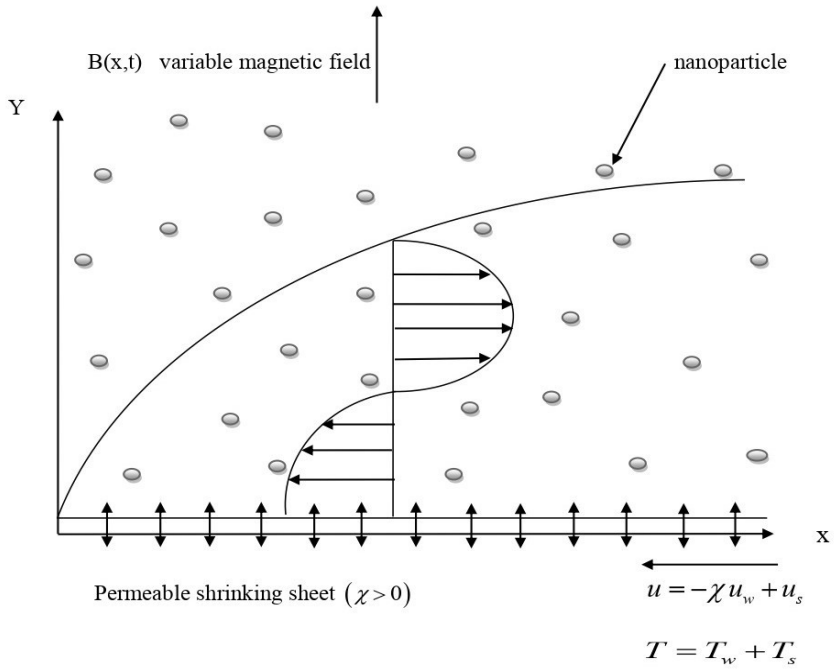

***Figure* 2.1:** Physical model and the coordinate system.

$$\frac{\mu_f}{(\rho C)_f}\left(\frac{\partial u}{\partial y}\right)^2 + \frac{Q(T-T_\infty)}{(\rho C)_f}, \tag{2.3}$$

$$\frac{\partial C}{\partial t} + u\frac{\partial C}{\partial x} + v\frac{\partial C}{\partial y} = D_B\frac{\partial^2 C}{\partial y^2} + \frac{D_T}{T_\infty}\frac{\partial^2 T}{\partial y^2} - Cr\,(C - C_\infty) + \frac{D_m K_T}{T_m}\frac{\partial^2 T}{\partial y^2}, \tag{2.4}$$

Subject to the following boundary conditions:

$$t \le 0 : u = 0, v = 0, T = T_w; \tag{2.5}$$

u and v are function of x and t

$$t > 0 : u = -\chi u_w\,(x,t) + u_s, v = -v_w\,(x,t)\,, T = T_w + T_s, D_B\frac{\partial C}{\partial y} + \frac{D_T}{T_\infty}\frac{\partial T}{\partial y} = 0$$
$$at \quad y = 0;$$
$$u \to 0, v \to 0, \quad T \to T_\infty, \quad C \to C_\infty \quad as \quad y \to \infty, \tag{2.6}$$

here $\tau = \frac{(\rho C_p)_{np}}{(\rho C_p)_f}$ is ratio of nanoparticle heat capacity and the base fluid heat capacity, $\alpha_f = \frac{\kappa_f}{(\rho C_p)_f}$ is thermal diffusivity of the fluid, $K = K_0\left(\frac{x^{m-1}}{1-\lambda t}\right)^{-1}$ is permeability of the porous medium, $Q = Q_0\left(\frac{x^{m-1}}{1-\lambda t}\right)$ is heat generation, $Cr = Cr_0\frac{x^{m-1}}{1-\lambda t}$ is rate of chemical reaction. The variable magnetic field is $B\,(x,t) = B_0\left(\frac{x^{m-1}}{1-\lambda t}\right)^{\frac{1}{2}}$, where B_0 is constant. $u_s = L\frac{\partial u}{\partial y}$ is slip velocity, where $L\,(x,t) = L_1\left(\frac{x^{m-1}}{1-\lambda t}\right)^{-\frac{1}{2}}$ is velocity slip factor and $T_s = N\frac{\partial T}{\partial y}$ is thermal slip, where $N\,(x,t) = N_1\left(\frac{x^{m-1}}{1-\lambda t}\right)^{-\frac{1}{2}}$ is velocity slip factor.

By using Rosselands approximation, the radiative heat flux is

$$q_r = -\left(\frac{4}{3}\frac{\sigma^*}{k^*}\right)\frac{\partial T^4}{\partial y}, \tag{2.7}$$

where k^* is the absorption coefficient, σ^* is the Stefan-Boltzmann constant.The temperature difference is assuming such that T^4 may be expended in a Taylor series about T_∞ and neglecting higher order terms, we get

$$T^4 = 4T_\infty^3 T - 3{T_\infty}^4. \tag{2.8}$$

Using eq.(2.8) in eq.(2.7), we get

$$q_r = -\left(\frac{4}{3}\frac{\sigma^*}{k^*}\right)\frac{\partial}{\partial y}\left(4T_\infty^3 T - 3T_\infty{}^4\right) = -\frac{16}{3}\frac{\sigma^* T_\infty^3}{k^*}\frac{\partial T}{\partial y}$$

and hence

$$\frac{\partial q_r}{\partial y} = -\frac{16}{3}\frac{\sigma^* T_\infty^3}{k^*}\frac{\partial^2 T}{\partial y^2}. \tag{2.9}$$

In terms of the stream function the velocity components are:

$$u = \frac{\partial \psi}{\partial y}, v = -\frac{\partial \psi}{\partial x}. \tag{2.10}$$

Now, using the similarity transformations

$$\eta = y\sqrt{\left(\frac{u_w(x,t)}{x\nu_f}\right)}, \psi = \sqrt{\nu_f x u_w(x,t)} f(\eta),$$
$$\theta(\eta) = \frac{T-T_\infty}{T_w-T_\infty}, \phi(\eta) = \frac{C-C_\infty}{C_\infty}, \tag{2.11}$$

equations (2.1) to (2.6) reduce to

$$f''' + \left(\frac{m+1}{2}\right) f f'' - m f'^2 - A\left(f' + \frac{\eta}{2} f''\right) - \left(Ha^2 + K^*\right) f' = 0, \tag{2.12}$$

$$\frac{1}{Pr_{eff}}\theta'' + \left(\frac{m+1}{2}\right) f\theta' + Nb\theta'\phi' + Nt\theta'^2 - \frac{A}{2}\eta\theta' + Ecf''^2 + Q^*\theta = 0, \tag{2.13}$$

$$\phi'' + \left(\frac{m+1}{2}\right) Lef\phi' + \frac{Nt}{Nb}\theta'' - LeCr^*\phi - \frac{\eta}{2} LeA\phi' + LeSr\theta'' = 0, \tag{2.14}$$

with the boundary conditions

$$\eta = 0 : f(\eta) = S, f'(\eta) = -\chi + \lambda^* f''(\eta), \theta(\eta) = 1 + \delta\theta'(\eta), Nb\phi'(\eta) + Nt\theta'(\eta) = 0;$$

$$\eta \to \infty : f'(\eta) \to 0, \theta(\eta) \to 0, \phi(\eta) \to 0. \tag{2.15}$$

The parameters used in equations (2.12) to (2.15) are as follows:

$$Pr_{eff} = \frac{Pr}{(1+R)}, Pr = \frac{\nu_f}{\alpha_f}, Le = \frac{\nu_f}{D_B}, Nb = \frac{\tau D_B C_\infty}{\nu_f}, R = \frac{16}{3}\frac{\sigma^* T_\infty^3}{\kappa_f k^*}, Nt = \frac{\tau D_T (T_w - T_\infty)}{\nu_f T_\infty},$$
$$Ha^2 = \frac{\sigma B_0^2}{\rho_f a}, K^* = \frac{\nu_f}{K_0 a}, Q^* = \frac{Q_0 \alpha_f}{\kappa_f a}, Cr^* = \frac{Cr_0}{a}, A = \frac{\lambda}{a x^{m-1}}, Ec = \frac{u_w^2}{(C_p)_f (T_w - T_\infty)},$$
$$Sr = \frac{D_m K_T (T_w - T_\infty)}{\nu_f T_m C_\infty}, \lambda^* = L_1\sqrt{\frac{a}{\nu_f}}, S = \frac{2v_0}{\sqrt{a\nu_f}(m+1)}, \delta = N_1\sqrt{\frac{a}{\nu_f}}.$$

Here Pr_{eff} denote effective Prandlt number.
In this study, the important physical quantities are the skin friction coefficient and the local Nusselt number, which are defined as

$$C_{fx} = \frac{\tau_w}{\rho_f u_w^2(x,t)}, Nu_x = \frac{x q_w}{\kappa_f (T_w - T_\infty)}, \tag{2.16}$$

$$where \quad \tau_w = \mu_f\left(\frac{\partial u}{\partial y}\right)_{y=0} \quad and \quad q_w = -\left[\left(\kappa_f + \frac{16}{3}\frac{\sigma^* T_\infty^3}{k^*}\right)\frac{\partial T}{\partial y}\right]_{y=0}, \tag{2.17}$$

are the wall shear stress and the wall heat flux, respectively.
Using equations (2.11) and (2.17) into equation (2.16), we have

$$C_{fx} Re_x^{\frac{1}{2}} = f''(0) \quad and \quad Nu_x Re_x^{-\frac{1}{2}} = -(1+R)\theta'(0), \tag{2.18}$$

where $Re_x = \frac{u_w x}{\nu_f}$ is the local Reynolds number.

3 Numerical Solution

In this study, similarity transformations are used to reduce the governing equations (2.1) - (2.4) into a system of coupled non-linear ordinary differential equations (2.12)-(2.14) with boundary conditions. The coupled non-linear ordinary differential equations (2.12)-(2.14) are third order in f and second order in both θ and ϕ. These coupled equations are reduced to a system of seven simultaneous differential equations of first order with seven unknowns. To solve this system of equations using the Runge-kutta fourth order method, we need seven initial conditions. We already know two initial conditions in f and one initial condition in each of θ and ϕ. Also, the value of f', θ and ϕ are known at $\eta \to \infty$. Thus, these three end conditions can be utilize to produce three unknown initial conditions at $\eta = 0$ by using shooting technique. After knowing all the seven initial conditions, we solve this system of equations using fourth order Runge-Kutta integration scheme with the help of *MATLAB* software.

The equations (2.12)-(2.14) can be expressed as

$$f = f_1,$$

$$f_1{}' = f_2,$$

$$f_2{}' = f_3,$$

$$f_3{}' = -\left(\frac{m+1}{2}\right) f_1 f_3 + m f_2^2 + A\left(f_2 + \frac{\eta}{2} f_3\right) + \left(Ha^2 + K^*\right) f_2,$$

$$\theta = f_4,$$

$$f_4{}' = f_5,$$

$$f_5{}' = -Pr_{eff}\left[\left(\frac{m+1}{2}\right) f_1 f_5 + Nb f_5 f_7 + Nt f_5^2 - \frac{A}{2}\eta f_5 + Ec f_3^2 + Q^* f_4\right],$$

$$\phi = f_6,$$

$$f_6{}' = f_7,$$

$$f_7{}' = \left(\frac{Nt}{Nb} + LeSr\right)\left[Pr_{eff}\left(\left(\frac{m+1}{2}\right) f_1 f_5 + Nb f_5 f_7 + Nt f_5^2 - \frac{A}{2}\eta f_5 + Ec f_3^2 + Q^* f_4\right)\right] - \left(\frac{m+1}{2}\right) Le f_1 f_7 + LeCr^* f_6 + \frac{\eta}{2} LeA f_7,$$

with reduced boundary conditions

$$\eta = 0 : f_1 = S, f_2 = -\chi + \lambda^* f_3, f_4 = 1 + \delta f_5, f_7 = -\frac{Nt}{Nb} f_5;$$

$$\eta \to \infty : f_2 \to 0, f_4 \to 0, f_6 \to 0.$$

In this study, the boundary value problem is first converted into an initial value problem (*IVP*). Then, the *IVP* is solved by appropriate guessing of the missing initial value by the shooting method for several sets of parameters. The obtained results have been discussed and shown graphically and in tables.

4 Results and discussion

The non-dimensional equations (2.12)-(2.14) with boundary conditions (2.15) are solved numerically by Runge-kutta fourth order method with shooting technique. For numerical computation, we consider the non-dimensional parameter's values as $0 \le K^* \le 4.0$, $0 \le Ha^2 \le 1.5$, $0.01 \le Nt \le 1.0$, $0.1 \le Cr^* \le 7.0$, $0.5 \le Nb \le 10.0$, $0.1 \le Ec \le 1.0$, $4.0 \le Pr_{eff} \le 15.0$, $0.0 \le A \le 1.2$, $3.0 \le S \le 5.0$, $0.0 \le \lambda^* \le 0.2$, $5.0 \le Le \le 30.0$, $1.0 \le m \le 3.0$, $0.1 \le Q^* \le 10.0$, $0.0 \le R \le 1.04$, $0.05 \le Sr \le 0.20$, $0.1 \le \delta \le 0.2$, and $1.0 \le \chi \le 1.5$. The numerical values of parameters are fixed as given below: $K^* = 1.0$, $Ha^2 = 0.5$, $Nt = Nb = 0.5$, $Ec = Cr^* = 0.1$, $Pr = 8.16$, $Pr_{eff} = 6.8$, $Q^* = 0.1$, $A = 0.5$, $S = 3.0$, $Le = 10$, $Sr = 0.05$, $\delta = 0.1$, $\chi = 1.0$, $R = 0.2$ and $\lambda^* = 0.1$, unless stated separately. In Figure 4.1, consequence of permeability parameter (K^*) on velocity profile is sketched. It is comprehended that rise in the value of permeability parameter increases the velocity profile. Figure 4.2 illustrates the effect of magnetic field parameter(Ha^2) on

the nanofluid velocity profile. It is observed that increase in magnetic field parameter increases the velocity profile. Figures 4.3-4.4 and Figures 4.5-4.6 show the influence of the change of the thermophoresis parameter (Nt) and Brownian motion parameter (Nb) on the temperature and concentration profiles, respectively. It is noticed that, as the thermophoresis parameter and Brownian motion parameter increases, the thermal boundary layer thickness increases. Here the thermal rise is reported since higher Brownian motion includes the random acceleration of the fluid particles which generates extra energy. Nanofluid concentration increases with an increase in thermophoresis parameter and decreases near the surface with an increase in Brownian motion parameter. Figure 4.7 shows the effect of chemical reaction parameter (Cr^*) on the concentration of the nanofluid. It is observed that concentration of the nanofluid is on decline for higher estimation of Cr^*. Figure 4.8 and Figure 4.9 are graphed to comprehend the effect on temperature and concentration profiles for various values of effective Prandtl number (Pr_{eff}). The numerical results show that the impact of increasing values of effective Prandtl number leads to decrease in temperature and nanofluid concentration profiles. An enhancement in Eckert number causes increase in temperature and nanofluid concentration profiles. This effect is shown in Figure 4.10 and figure 4.11. Figure 4.12 shows the variation of velocity profile in response to a change in the values of unsteadiness parameter (A). It is seen that, as unsteadiness parameter increases, velocity increases. Figures 4.13-4.15 represent the effect of the suction parameter(S) on velocity, temperature and nanofluid concentration profiles, respectively. These plots show that velocity profile increases while temperature and nanofluid concentration profiles decrease with increasing value of suction parameter. Figures 4.16-4.18 illustrate the effect of the velocity slip parameter (λ^*) on velocity, temperature and concentration profiles, respectively. It is observed by Figure 4.16 that the velocity profile increases with increasing value of λ^* while Figure 4.17 and Figure 4.18 show that the velocity slip parameter affects the temperature and nanofluid concentration in an opposite manner. Figure 4.19 and Figure 4.20 show the impact of Lewis number (Le) on temperature and concentration distribution. It is seen by Figure 4.19 that temperature profile increases near the surface and reverses far from the surface with the increasing values of Le. From Figure 4.20, it is found that the nanoparticle concentration is a decreasing function of Le. Thinner concentration boundary layer and weaker mass diffusivity are proportional to increase in Le. Figures 4.21 and 4.22 show the effect of heat generation parameter (Q^*) on temperature and nanofluid concentration profiles and declare that, the temperature and concentration profiles increase with increasing value of heat generation parameter. Figure 4.23 and Figure 4.24 illustrate the effect of thermal slip parameter (δ) on the nanofluid temperature and concentration profiles. It can be seen that both nanofluid temperature and concentration profiles decrease with increasing values of thermal slip parameter. Figures 4.25-4.27 are plotted to analyze the behavior of $f^{'}(\eta)$, $\theta(\eta)$ and $\phi(\eta)$ for various values of χ. It is observed by Figure 4.25 that velocity has decreasing tendency with decreasing value of χ. It can also be noted by Figure 4.26 and Figure 4.27 that temperature and nanofluid concentration have increasing tendency with decreasing values of χ. The effect of power-law index (m) on velocity, temperature and nanoparticle volume fraction is drawn in Figures 4.28-4.30, respectively. It is observed that temperature and nanofluid concentration decrease while velocity profile increases with the increasing values of m. This is due to the fact that increment in power-law index (m) enhances the intensity of the cold fluid at the ambient towards the hot fluid near the sheet. This decreases the fluid temperature near the shrinking sheet. Figure 4.31 and Figure 4.32 outline the temperature and nanofluid concentration in the presence of the Soret number Sr. An increase in Sr increases the temperature and concentration profiles within the boundary layer. Figure 4.33 and Figure 4.34 show the effect of radiation absorption parameter (R). Temperature and concentration profiles increse with increase in radiation absorption parameter (R). The effect of various governing parameters on Skin friction and Nusselt number are calculated numerically and also presented in Table 4.1,4.2 and 4.3. From Table 4.1, it is clear that Skin friction increases for increasing value of parameters K^*, Ha^2, A, S and m while it is a decreasing function of parameters λ^* and χ. Also from Table 4.2 and 4.3, it is noted that the Nusselt number increases for increasing value of parameters Pr_{eff}, Cr^*, S, m and λ^* while it is a decreasing function of parameters K^*, Ha^2, Nt, Nb, Le, Ec, A, Sr, Q^*, χ, R and δ.

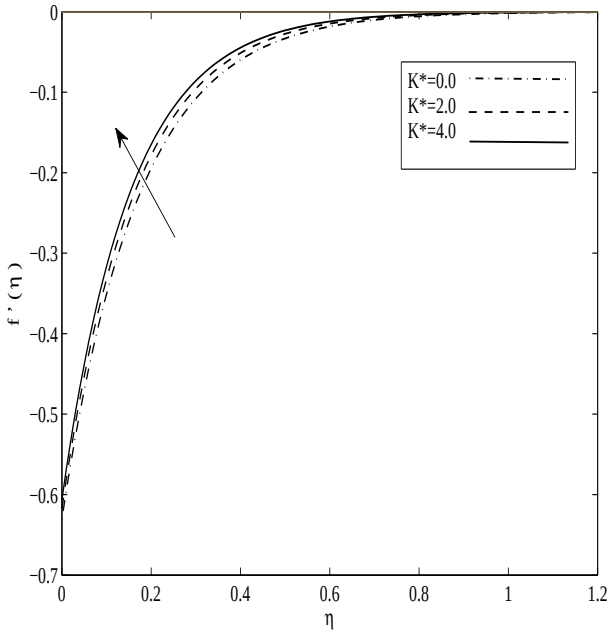

***Figure* 4.1:** Velocity behaviour for various values of K^*.

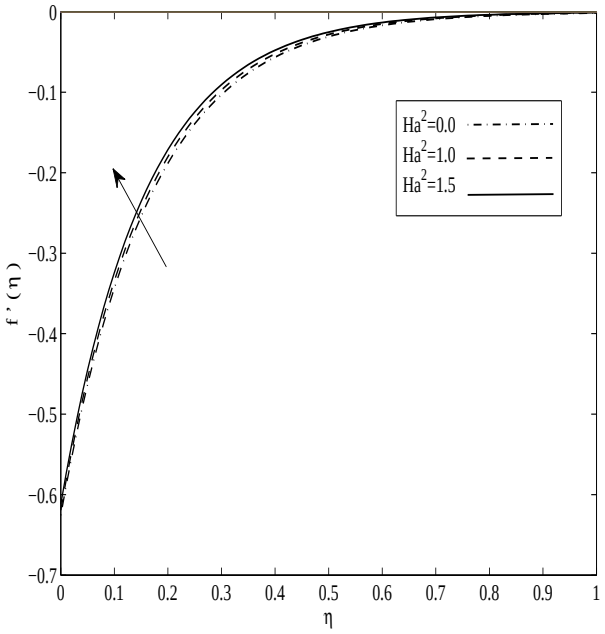

***Figure* 4.2:** Velocity behaviour for various values of Ha^2.

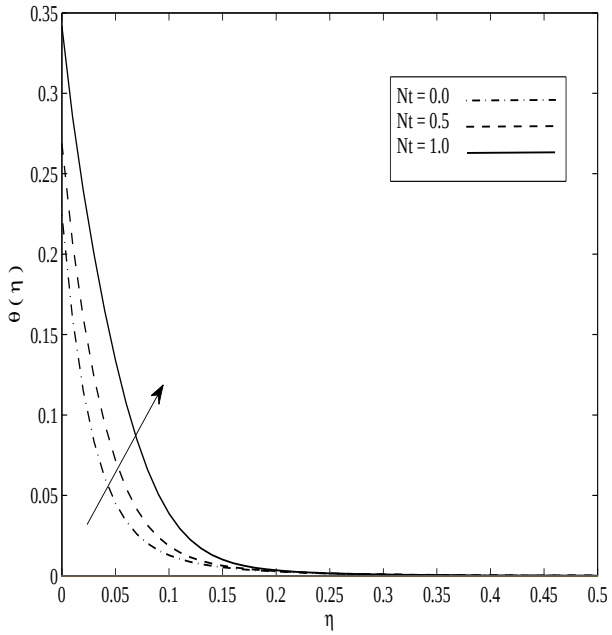

***Figure* 4.3:** Temperature behaviour for various values of Nt.

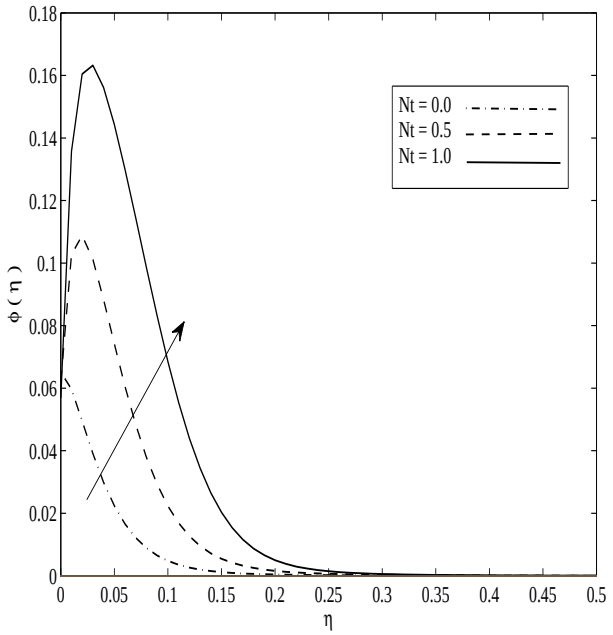

***Figure* 4.4:** Concentration behaviour for various values of Nt.

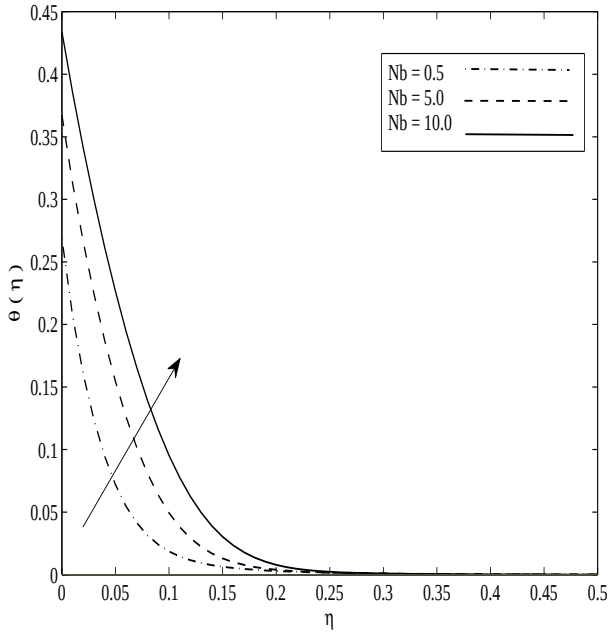

***Figure* 4.5:** Temperature behaviour for various values of Nb.

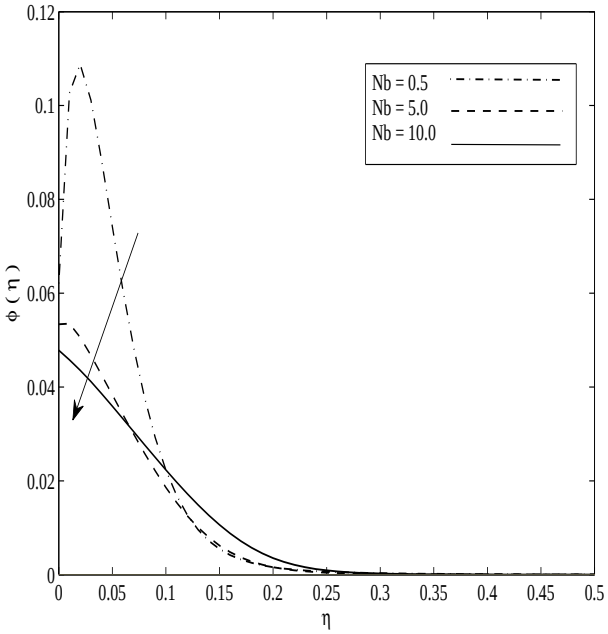

***Figure* 4.6:** Concentration behaviour for various values of Nb.

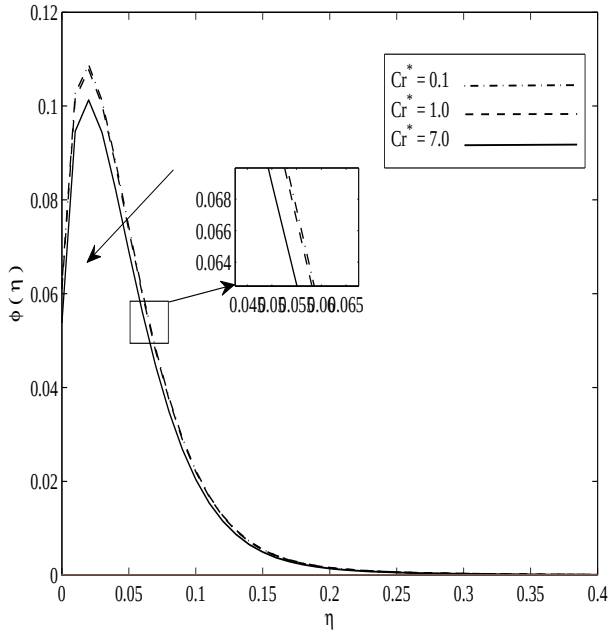

***Figure* 4.7:** Concentration behaviour for various values of Cr^*.

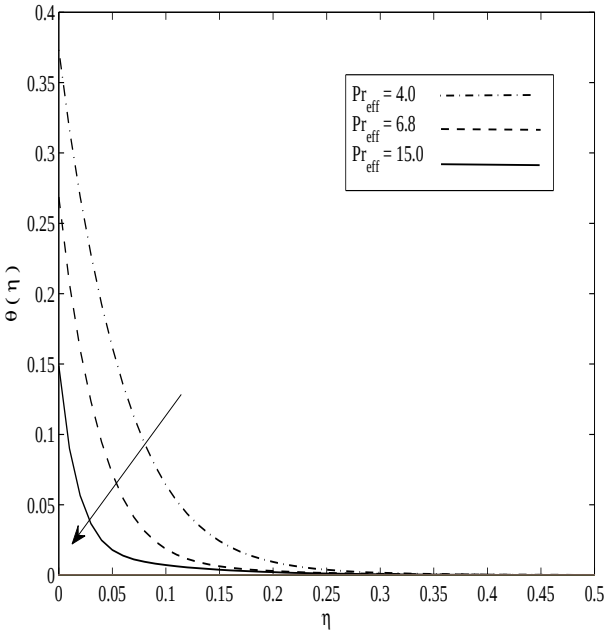

***Figure* 4.8:** Temperature behaviour for various values of Pr_{eff}.

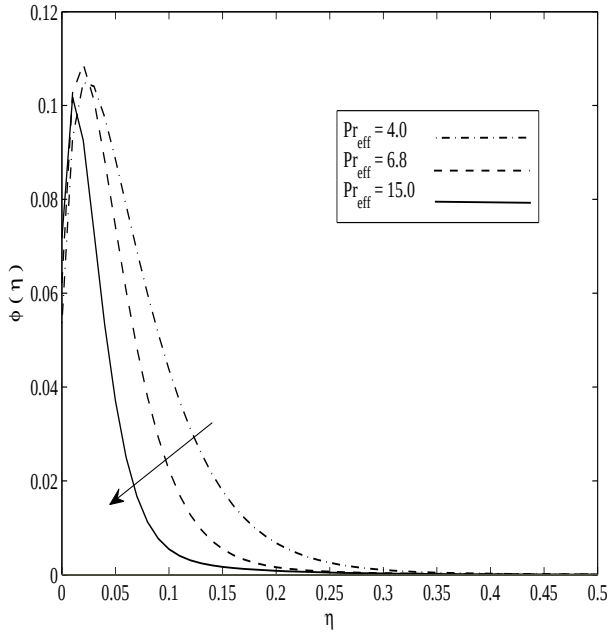

***Figure* 4.9:** Concentration behaviour for various values of Pr_{eff}.

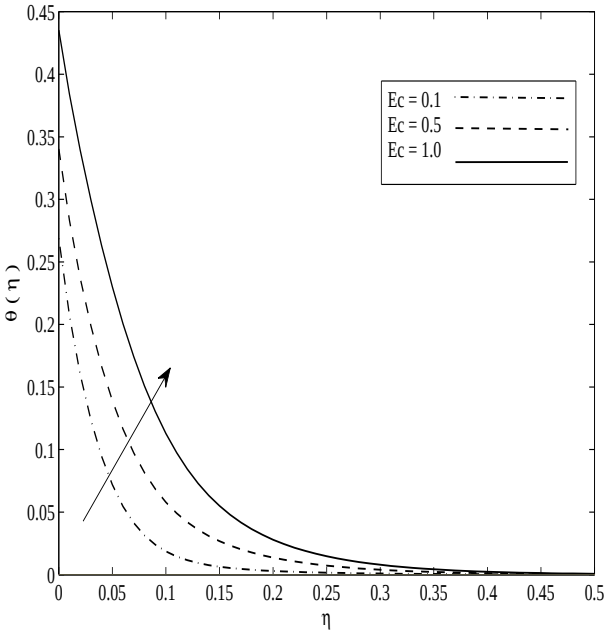

***Figure* 4.10:** Temperature behaviour for various values of Ec.

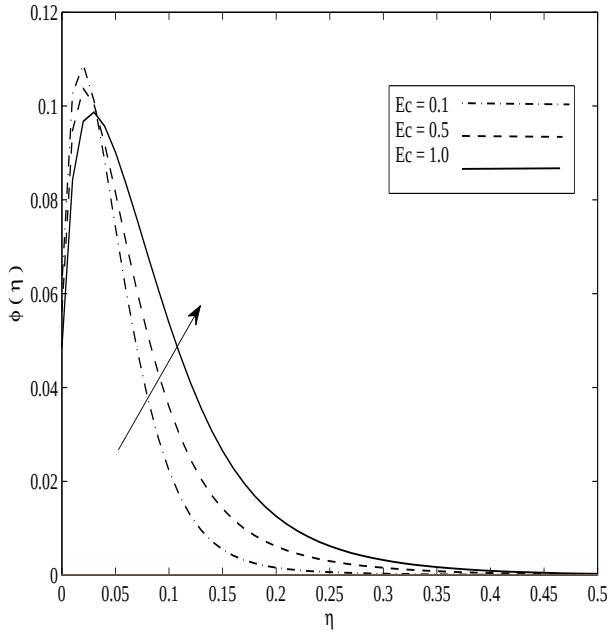

***Figure* 4.11:** Concentration behaviour for various values of Ec.

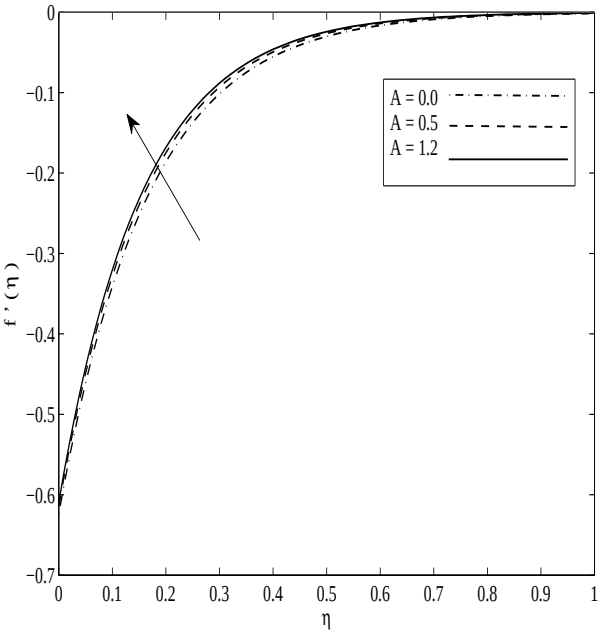

***Figure* 4.12:** Velocity behaviour for various values of A.

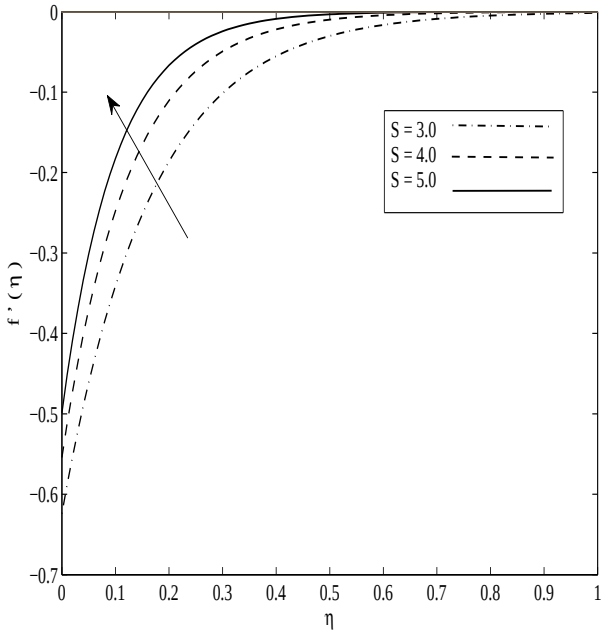

***Figure* 4.13:** Velocity behaviour for various values of S.

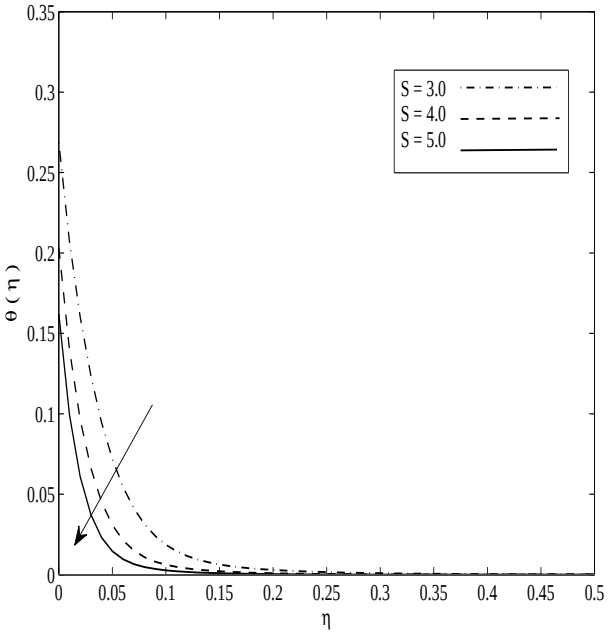

***Figure* 4.14:** Temperature behaviour for various values of S.

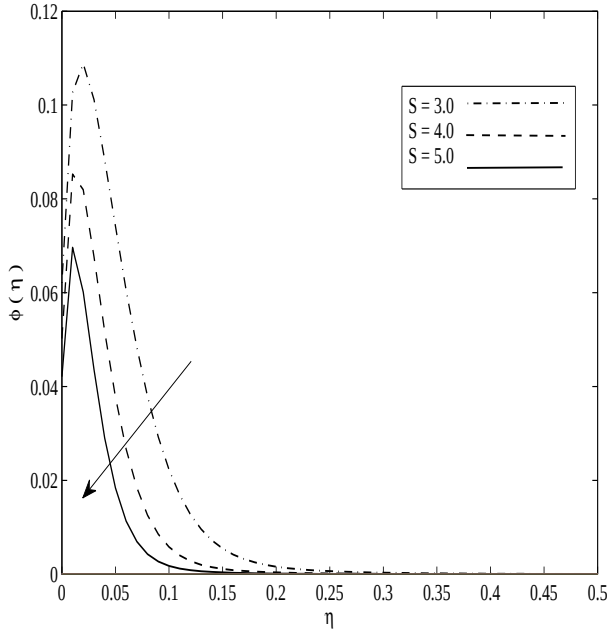

***Figure* 4.15:** Concentration behaviour for various values of S.

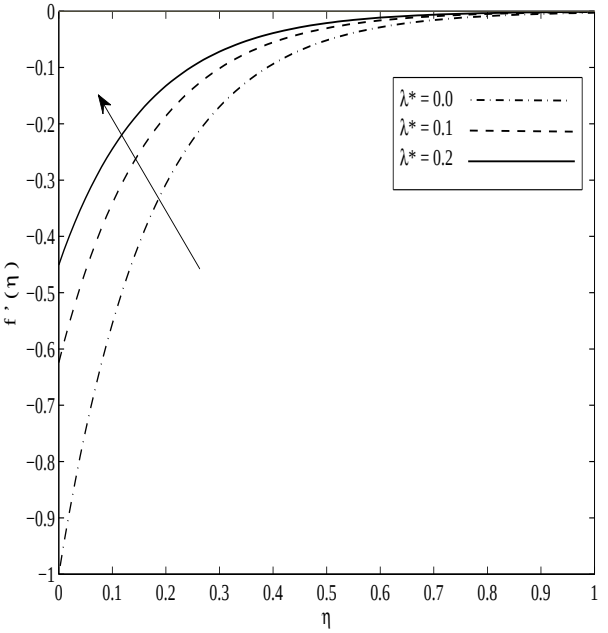

***Figure* 4.16:** Velocity behaviour for various values of λ^*.

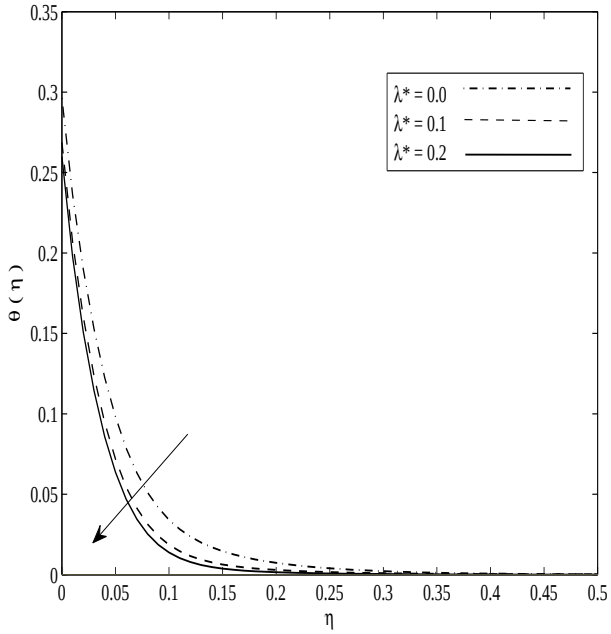

***Figure* 4.17:** Temperature behaviour for various values of λ^*.

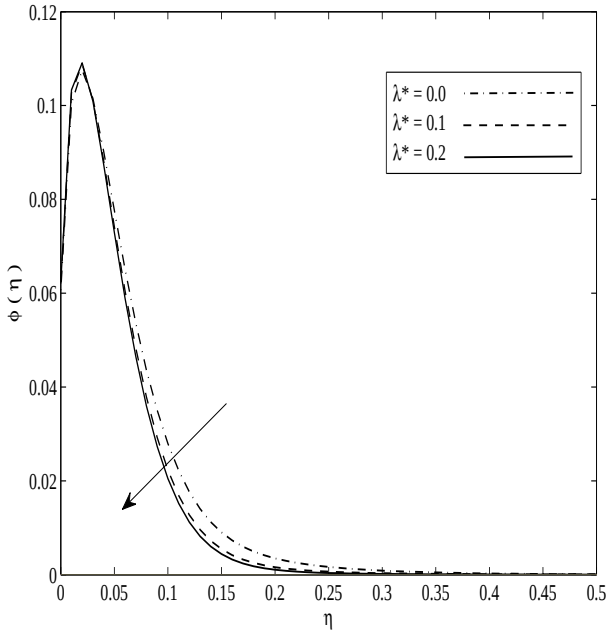

***Figure* 4.18:** Concentration behaviour for various values of λ^*.

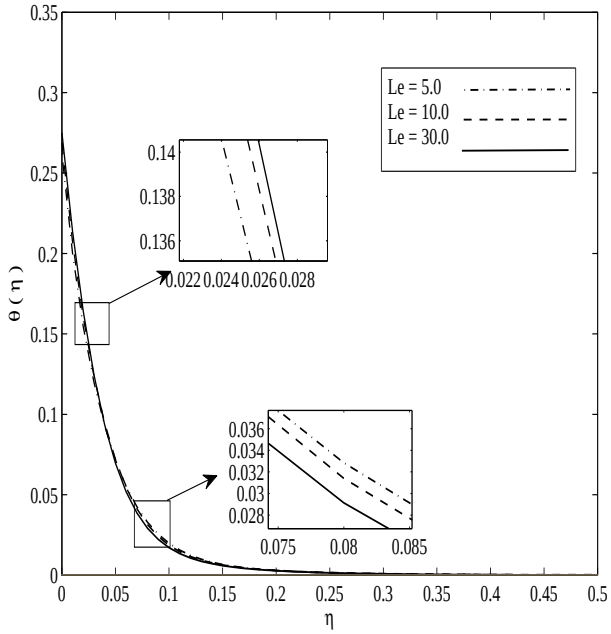

***Figure* 4.19:** Temperature behaviour for various values of Le.

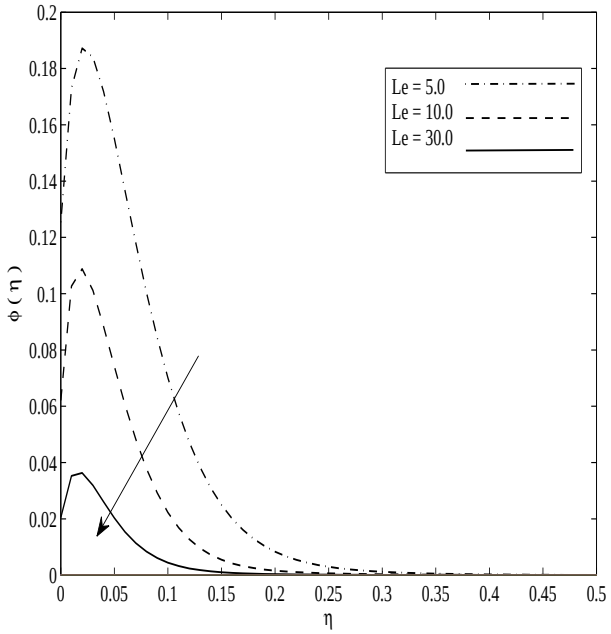

***Figure* 4.20:** Concentration behaviour for various values of Le.

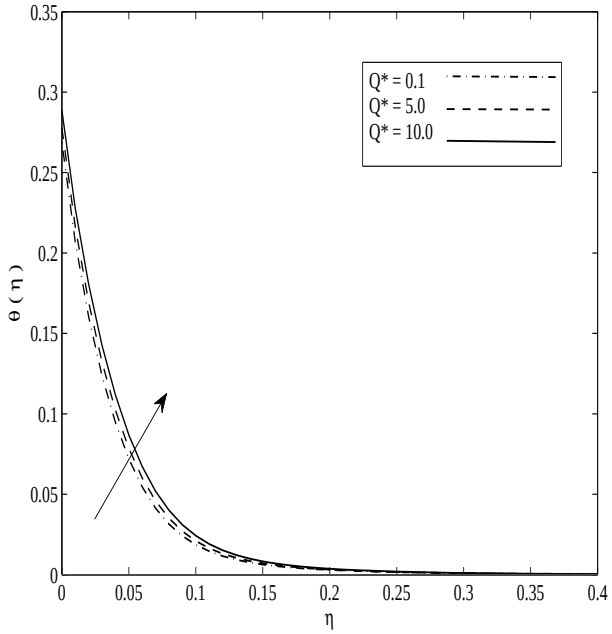

***Figure* 4.21:** Temperature behaviour for various values of Q^*.

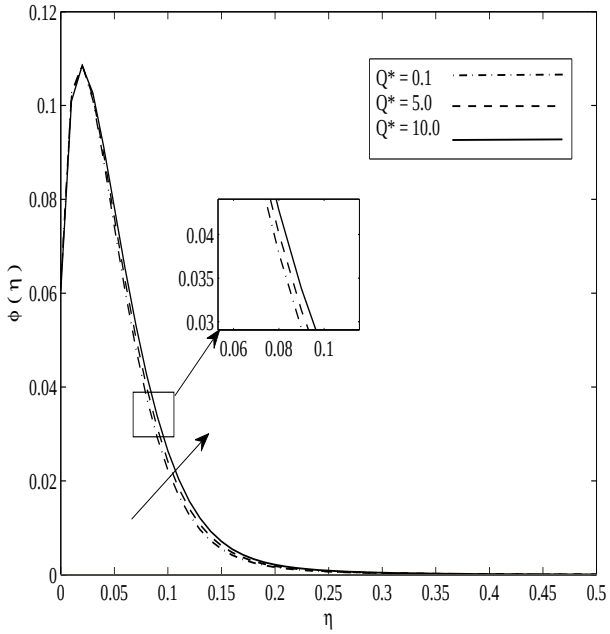

***Figure* 4.22:** Concentration behaviour for various values of Q^*.

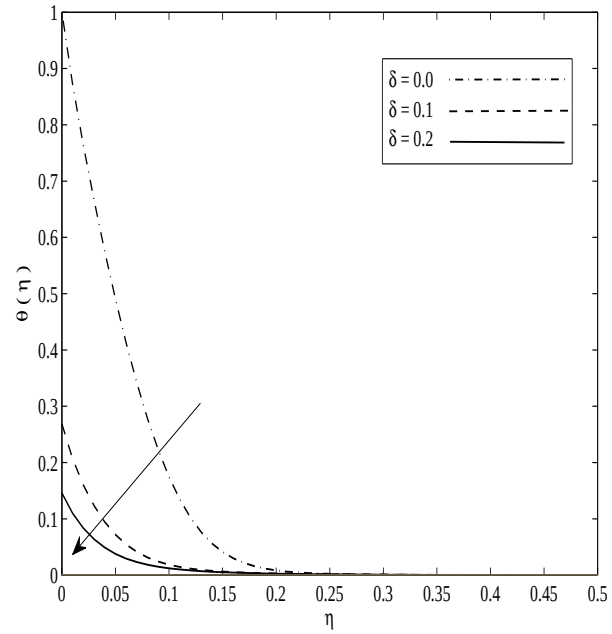

***Figure* 4.23:** Temperature behaviour for various values of δ.

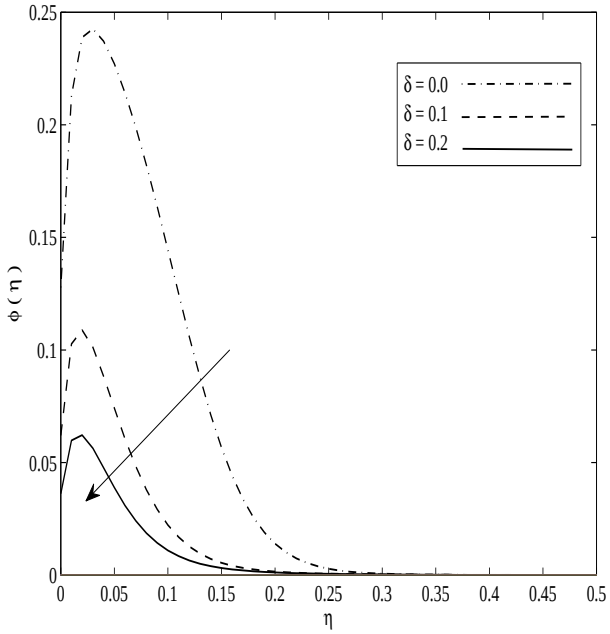

***Figure* 4.24:** Concentration behaviour for various values of δ.

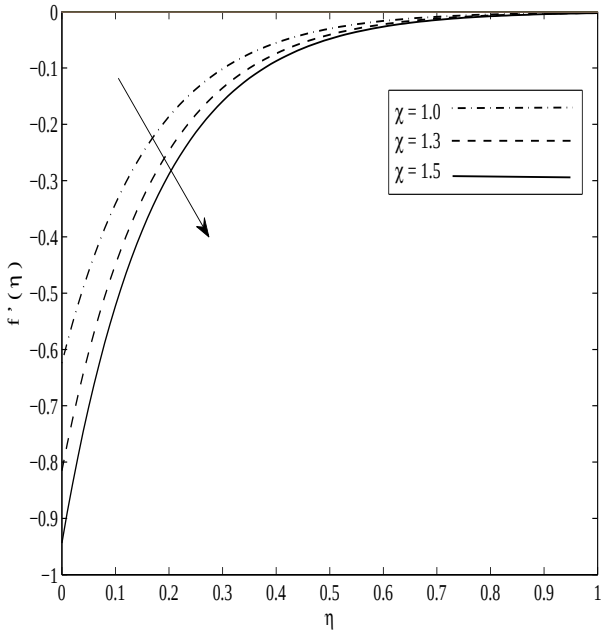

***Figure* 4.25:** Velocity behaviour for various values of χ.

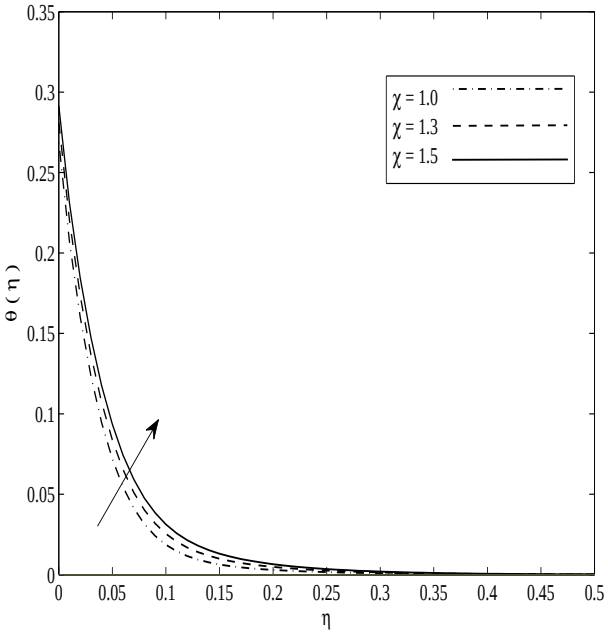

***Figure* 4.26:** Temperature behaviour for various values of χ.

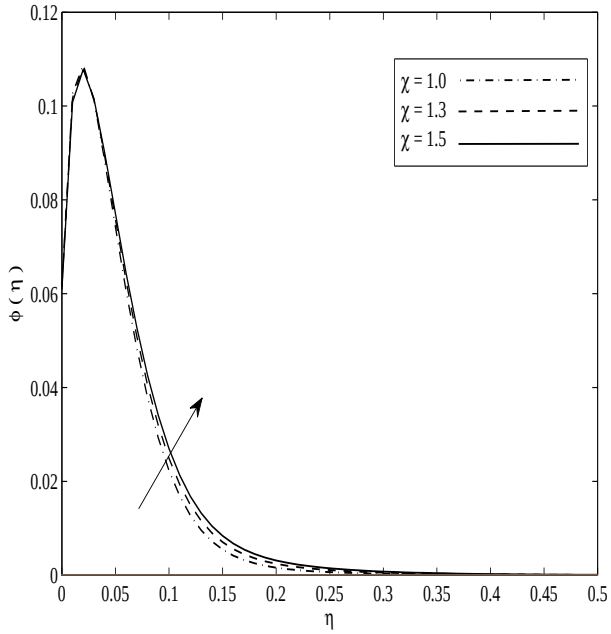

***Figure* 4.27:** Concentration behaviour for various values of χ.

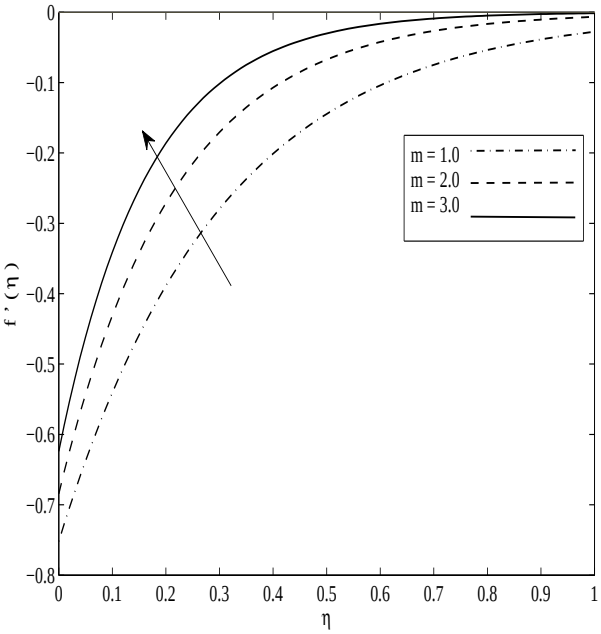

***Figure* 4.28:** Velocity behaviour for various values of m.

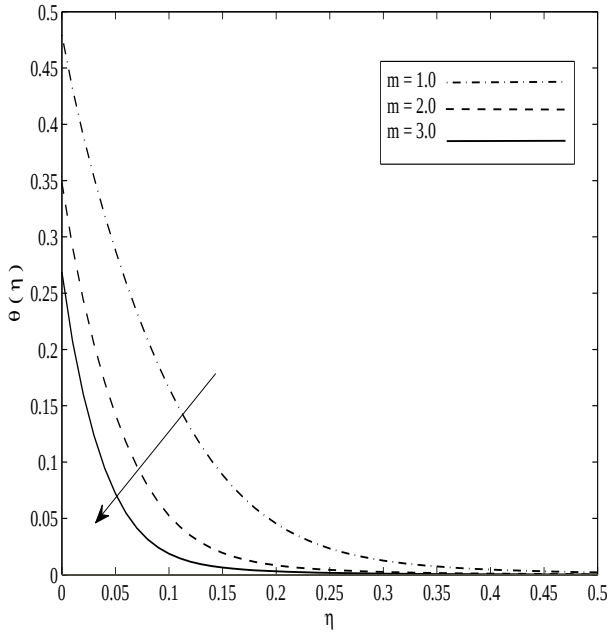

***Figure* 4.29:** Temperature behaviour for various values of m.

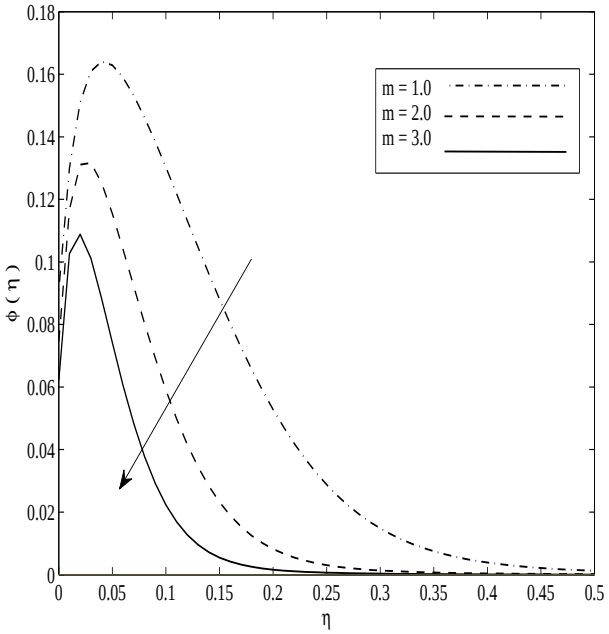

***Figure* 4.30:** Concentration behaviour for various values of m.

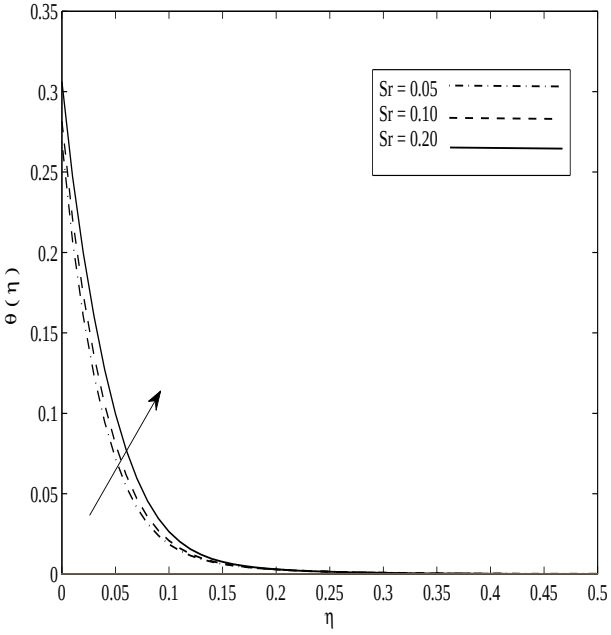

***Figure* 4.31:** Temperature behaviour for various values of Sr.

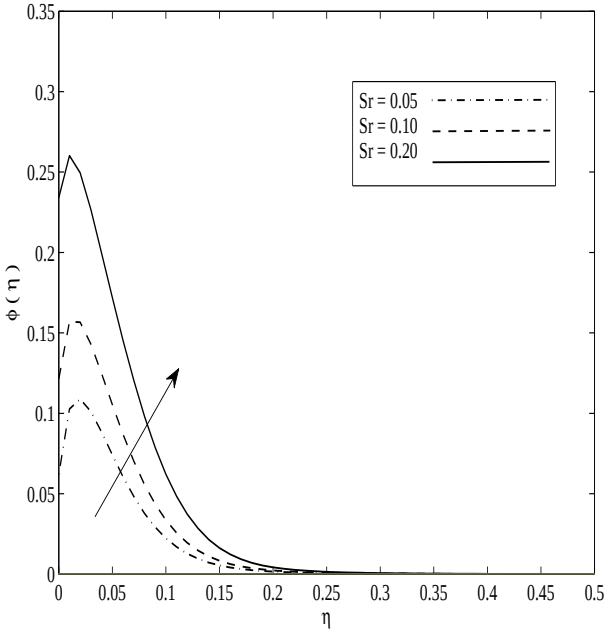

***Figure* 4.32:** Concentration behaviour for various values of Sr.

***Table* 4.1:** Numerical values of $C_{fx}Re_x^{1/2}$

K^*	Ha^2	A	S	λ^*	m	χ	$C_{fx}\ Re_x^{1/2}$
0.00	0.50	0.50	3.00	0.10	3.00	1.00	3.676558
1.00	**0.50**	**0.50**	**3.00**	**0.10**	**3.00**	**1.00**	**3.746045**
2.00							3.810179
4.00							3.925633
1.00	**0.00**	0.50	3.00	0.10	3.00	1.00	3.729214
	1.00						3.794596
	1.50						3.869821
1.00	0.50	**0.00**	3.00	0.10	3.00	1.00	3.728988
		1.20					3.769732
1.00	0.50	0.50	**4.00**	0.10	3.00	1.00	4.448826
			5.00				5.006289
1.00	0.50	0.50	3.00	**0.00**	3.00	1.00	5.828953
				0.20			2.739946
1.00	0.50	0.50	3.00	0.10	**1.00**		2.445871
					2.00		3.135196
1.00	0.50	0.50	3.00	0.10	3.00	**1.30**	4.828288
						1.50	5.537819

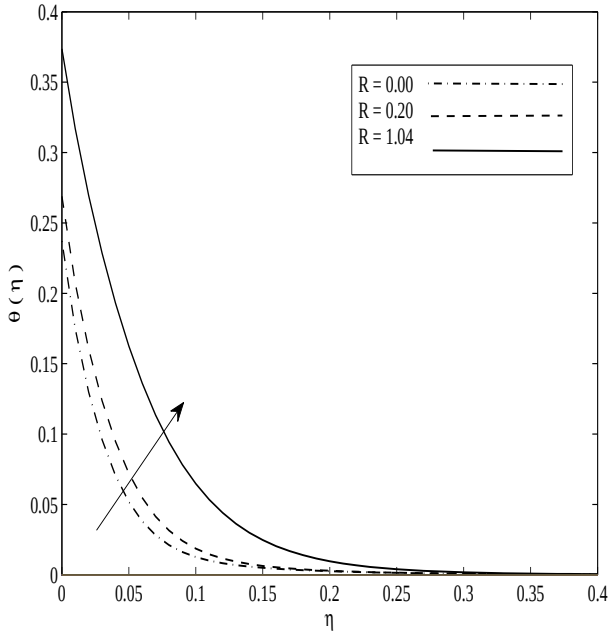

***Figure* 4.33:** Temperature behaviour for various values of R.

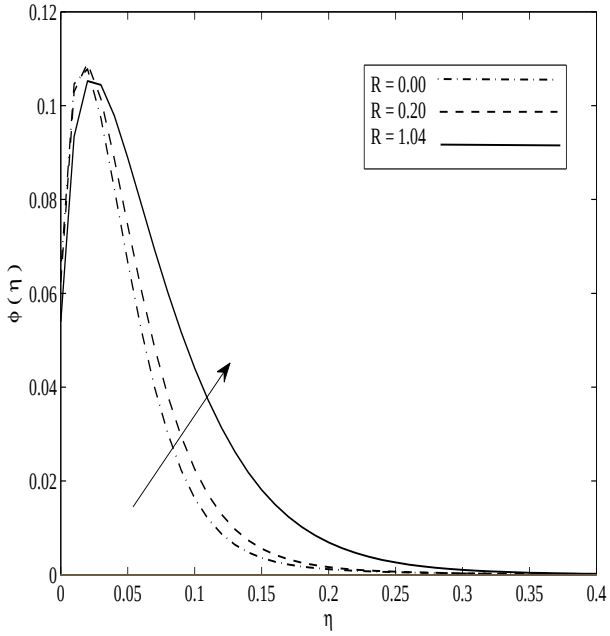

***Figure* 4.34:** Concentration behaviour for various values of R.

.

5 Conclusions

The numerical investigation has been carried out to analyze the Soret effect on *MHD* nanofluid flow past a nonlinear shrinking sheet in the presence of thermal radiation, viscous dissipation and chemical reaction under

***Table* 4.2:** Numerical values of $Nu_x Re_x^{-1/2}$

K^*	Ha^2	Nt	Nb	Ec	Cr^*	Pr_{eff}	Le	$Nu_x Re_x^{-1/2}$
0.00	0.50	0.50	0.50	0.10	0.10	6.80	10.0	8.776111
1.00	**0.50**	**0.50**	**0.50**	**0.10**	**0.10**	**6.80**	**10.0**	**8.773807**
2.00								8.772007
4.00								8.768707
1.00	**0.00**	0.50	0.50	0.10	0.10	6.80	10.0	8.774323
	1.00							8.772523
	1.50							8.770087
1.00	0.50	**0.00**	0.50	0.10	0.10	6.80	10.0	9.306258
		1.00						7.895671
1.00	0.50	0.50	**5.00**	0.10	0.10	6.80	10.0	7.586038
			10.00					6.785098
1.00	0.50	0.50	0.50	**0.50**	0.10	6.80	10.0	7.914547
				1.00				6.778293
1.00	0.50	0.50	0.50	0.10	0.10	**4.00**		7.516687
						15.00		10.216327
1.00	0.50	0.50	0.50	0.10	0.10	6.80	**5.00**	8.854783
							30.0	8.696666
1.00	0.50	0.50	0.50	0.10	**1.00**	6.80	10.0	8.776197
					7.00			8.788108

***Table* 4.3:** Numerical values of $Nu_x Re_x^{-1/2}$

S	λ^*	m	Sr	A	R	Q^*	δ	χ	$Nu_x Re_x^{-1/2}$
3.00	**0.10**	**3.00**	**0.05**	**0.50**	**0.20**	**0.10**	**0.10**	**1.00**	**8.773807**
4.00	0.10	3.00	0.05	0.50	0.20	0.10	0.10	1.00	9.558962
5.00									10.053549
3.00	**0.00**	3.00	0.05	0.50	0.20	0.10	0.10	1.00	8.445462
	0.20								8.877429
3.00	0.10	**1.00**	0.05	0.50	0.20	0.10	0.10	1.00	6.230143
		2.00							7.816951
3.00	0.10	3.00	**0.10**	0.50	0.20	0.10	0.10	1.00	8.617619
			0.20						8.321183
3.00	0.10	3.00	0.05	0.50	0.20	**5.00**	0.10	1.00	8.662975
						10.00			8.256715
3.00	0.10	3.00	0.05	0.50	0.20	0.10	**0.00**	1.00	17.873911
							0.20		5.124427
3.00	0.10	3.00	0.05	0.50	0.20	0.10	0.10	**1.30**	8.623513
								1.50	8.501317
3.00	0.10	3.00	0.05	**0.00**	0.20	0.10	1.10	1.00	8.778535
				1.20					8.767389
3.00	0.10	3.00	0.05	0.50	**0.00**	0.10	0.10	1.00	7.629306
					1.04				12.778368

velocity and thermal slip conditions. The influence of the governing parameters on velocity, temperature and concentration profiles has been numerically evaluated using Runge- Kutta fourth order method with shooting technique in *MATLAB* software. Some of the important results are as follows:

- Velocity profiles increase for permeability parameter (K^*) and velocity slip parameter (λ^*) while decrease for shrinking parameter (χ).
- The surface temperature increases with an increase in the values of the governing parameters, such as Brownian motion parameter (Nb), thermophoresis parameter (Nt), heat generation parameter (Q^*), shrinking parameter (χ) and Lewis number (Le).
- The enhancement in chemical reaction parameter (Cr^*) declines the nanofluid concentration profile while the nanofluid concentration profile rises up with Soret number (Sr).
- An increase in suction parameter (S) increases both the Skin friction and local Nusselt number.
- Skin friction decreases whereas Nusselt number increases with increasing value of velocity slip parameter (λ^*) whereas reverse effect obtained with the permeability parameter (K^*), unsteadiness parameter (A), magnetic field parameter (Ha^2) and shrinking parameter (χ).
- The Nusselt number decreases with an increase of Brownian motion parameter (Nb), thermophoresis parameter (Nt), heat generation parameter (Q^*), thermal slip parameter (δ), Eckert number (Ec) and Soret number (Sr).

Acknowledgement: Authors are very much grateful to the Editors and Reviewers for their fruitful suggations to bring the paper in present form.

References

[1] I. Anwar, A. R. Qasim, Z. Ismail, M. Z. Salleh and S. Shafie, Chemical reaction and uniform heat generation or absorption effects on MHD stagnation-point flow of a nanofluid over a porous sheet, *World Applied Science Journal*, **24** (10)(2013), 1390-1398.

[2] K. S. Awang and I. Hashim, Series solution of flow over nonlinearly stretching sheet with chemical reaction and magnetic field, *Physics Letters A*, **372**(2008), 2258-2263.

[3] A. Badr and A. M. Subhas, MHD boundary layer flow over a nonlinear stretching sheet in a nanofluid with convective boundary condition, *Journal of Computational and Theoretical Nanoscience*, **12**(12)(2015), 6020-6027.

[4] J. Buongiorno, Convective transport in nanofluids, *ASME Journal of Heat Transfer*, **128**(2006), 240-250.

[5] L.J. Crane, Flow past a stretching plate, *Journal of Applied Mathematics and Physics*, **21**(4)(1970), 645-647.

[6] S. U. S. Choi and J. A. Eastman, Enhancing thermal conductivity of fluids with nanoparticles, *American Society of Mechanical Engineers, Fluids Engineering Division*, **231**(1995), 99-105.

[7] S. Das, R. N. Jana, and O. D. Makinde, MHD Boundary Layer slip flow and heat transfer of nanofluid past a vertical stretching sheet with Non-uniform heat generation/absorption, *International Journal of Nanoscience*, **13**(3)(2014), 1450019(1-12).

[8] Y.S. Daniel, Z.A. Aziz, Z. Ismail and F. Salah, Effects of slip and convective conditions on MHD flow of nanofluid over a porous nonlinear stretching/shrinking sheet, *Australian Journal of Mechanical Engineering*, **16**(3)(2018), 213-219.

[9] K. Das, Nanofluid flow over a non-linear permeable stretching sheet with partial slip, *Journal of the Egyptian Mathematical Society*, **23**(2)(2015), 451-456.

[10] E. R. G. Eckert and R. M. Drake, Analysis of Heat and Mass Transfer, *Mc-Graw Hill*, New York (1972).

[11] T. Fang and J. Zhang, Closed-form exact solution of MHD viscous flow over a shrinking sheet. *Communications in Nonlinear Science and Numerical Simulation*, **14**(2009), 2853-2857.

[12] F. M. Hady, F. S. Ibrahim, S.M. Abdel-Gaied and M.R. Eid, Radiation effect on viscous flow of a nanofluid and heat transfer over a nonlinearly stretching sheet. *Nanosccale Research Letters*, **7**(2012).

[13] M. A. A. Hamad, I. Pop and A. M. Ismail, Magnetic field effects on free convection flow of a nanofluid past a vertical semi-infinite flat plate, *Nonlinear Analysis: Real World Applications*, **12**(3)(2011), 1338-1346.

[14] A. V. Kuznetsov and D. A. Nield, Natural convection boundary-layer of a nanofluid past a vertical plate: a revised model, *International Journal Thermal Sciences*, **77**(2014), 126-129.

[15] M. Mustafa and J. A. Khan, Model for flow of Casson nanofluid past a non-linearly stretching sheet considering magnetic field effects, *AIP Advances*, **5**(2015), 077148.

[16] M. Mustafa ,J.A. Khan ,T. Hayat and A. Alsaedi, Boundary layer flow of nanofluid over a nonlinearly stretching sheet with convective boundary condition, *IEEE Transactions on Nanotechnology*, **14**(1)(2015), 159-168.

[17] O.D. Makinde and A. Aziz, Boundary layer flow of a nanofluid past a stretching sheet with a convective boundary condition, *International Journal Thermal Sciences*, **50**(7)(2011), 1326-1332.

[18] C. L. M. H. Navier, Memoire sur les lois du mouvement des fluids, *Mmoires de lAcadmie Royale des Sciences de lInstitut de France*, **6**(1823), 389-440.

[19] D. Pal, G. Mandal and K. Vajravelu, MHd convectiondissipation heat transfer over a non-linear stretching and shrinking sheets in nanofluids with thermal radiation, *International Journal of Heat and Mass Transfer*, **65**(2013), 481-490.

[20] K.V. Prasad, K. Vajravelu and P.S. Datti, The effects of variable fluid properties on the hydro-magnetic flow and heat transfer over a non-linearly stretching sheet, *International Journal of Thermal Sciences*, **49**(2010), 603-610.

[21] A. M. Rohini, S. Ahmad, A. I. M. Islam and I. Pop, Flow and heat transfer over an unsteady shrinking sheet with suction in a nanofluid using Boungiornos model, *International Communications in Heat and Mass Transfer*, **43**(2013), 75-80.

[22] D. Ramya, R. Srinivasa Raju and J. Anand Rao, Influence of Chemical Reaction on MHD boundary Layer flow of Nanofluids over a Nonlinear Stretching Sheet with Thermal Radiation, *Journal of Nanofluids*, **5**(2016), 880.

[23] D. Ramya, R. Srinivasa Raju,J. Anand Rao and M. M. Rashidi, Boundary layer viscous flow of nanofluids and heat transfer over a nonlinearly isothermal stretching sheet in the presence of Heat Generation/Absorption and slip boundary conditions, *International Journal of Nanoscience and Nanotechnology*, **12**(4)(2016),: 251-268.

[24] M. M. Rahman and I. A. Eltayeb, Radiative heat transfer in a Hydromagnetic nanofluid past a non-linear stretching surface with convective boundary condition, *Meccanica*, **48**(3)(2013), 601-615.

[25] M.M. Rashidi, N.V. Ganesh, A.A. Hakeem and B. Ganga, Buoyancy effect on MHD flow of nanofluid over a stretching sheet in the presence of thermal radiation, *Journal of Molecular Liquids*, **198**(2014), 234-238.

[26] P. B. A. Reddy, S. Suneetha and N. Bhaskar Reddy, Numerical study of MHD boundary layer slip flow of a Maxwell nanofluid over an exponentially stretching surface with convective boundary condition, *Propulsion and Power Research*, **6**(4)(2017), 259-268.

[27] P. Rana, R. Bhargava and O.A. Beg, Finite element simulation of unsteady magneto-hydrodynamic transport phenomena on a stretching sheet in a rotating nanofluid, *The Journal of Nanomaterials, Nanoengineering and Nanosystems*, **227**(2011), 77-99.

[28] P. Rana, R. Dhanai and L. Kumar, Radiative nanofluid flow and heat transfer over a non-linear permeable sheet with slip conditions and variable magnetic field: dual solutions, *Ain Shams Engineering Journal*, **8**(2017), 341-352.

[29] R. Ch. Reddy, P. V. S. N. Murthy, A. M. Rashad and J. Chamkha Ali, Soret effect on stagnation-point flow past a stretching/shrinking sheet in a nanofluid-saturated non- Darcy porous medium, *An International Journal of Special Topics and Reviews in Porous Media*,**7(3)**(2016), 229-243.

[30] M. A. Seddeek, Effects of radiation and variable viscosity on a MHD free convection flow past a semi-infinite flat plate with an aligned magnetic field in the case of unsteady flow, *International Journal of Heat and Mass Transfer*, **45**(2001), 931-935.

[31] M. Sheikholeslami and D. D. Ganji, Ferro hydrodynamic and magneto hydrodynamic effects on ferro fluid flow and convective heat transfer, *Energy*, **5**(2014), 400-410.

[32] M. Sheikholeslami and M. M. Rashidi, Effect of space dependent magnetic field on free convection of Fe_3O_4-water nanofluid, *Journal of the Taiwan Institute of Chemical Engineers*, **56**(2015), 6-15.

[33] M. Sheikholeslami, S. Soleimani and D.D. Ganji, Effect of electric field on hydrothermal behavior of nanofluid in a complex geometry, *Journal of Molecular Liquids*, **213**(2016), 153-161.

[34] N. Sandeep and C. Sulochana, MHD flow over a permeable stretching/shrinking sheet of a nanofluid with suction/injection, *Alexandria Engineering Journal*, **55**(2016), 819-827.

[35] S. Suneetha, K. Subbarayudu, L. Wahidunnisa and P. B. A. Reddy, Navier slip condition On Time-dependent radiating nanofluid with the Soret effect, *Engineering Transactions*, **(2)**(2020), 177-198.